High-Resolution Passive Video-Rate Imaging at 350 GHz*

Daniel Becker[a], Cale Gentry[b], Peter Ade[c], James Beall[a], Hsiao-Mei Cho[a], Simon Dicker[d], William Duncan[a†], Mark Halpern[e], Gene Hilton[a], Kent Irwin[a], Peter Lowell[a], Michael Niemack[a], Nick Paulter[a], Carl Reintsema[a], Frank Schima[a], Robert Schwall[a], Carole Tucker[c]

[a]NIST-Boulder

[b]University of Oklahoma

[c]Cardiff University

[d]University of Pennsylvania

[e]University of British Columbia

ABSTRACT

We are developing a 350 GHz cryogenic passive video imaging system for use in standoff security applications. This demonstration system uses 800 photon-noise-limited superconducting transition edge sensor bolometers, read out using a time-division multiplexed readout system. It will image a 1 m × 1 m field of view at a standoff distance of 16 m to a resolution of approximately 1 cm at video frame rates (20 frames per second). High spatial resolution is achieved by the use of an f/2.0 Cassegrain optical system with 1.3 m primary mirror. Preliminary dark and optical testing of prototype detectors indicates that we can achieve a noise equivalent temperature difference (NETD) below 100 mK for the fully sampled 1 m × 1 m image at 20 frames per second. We report on the current status of development of this system.

1. INTRODUCTION

Millimeter-wavelength radiation penetrates clothing well and is non-ionizing, making it a good candidate for identifying threats held beneath clothing.[1] For detection of threats at close distances in portal security scenarios, active millimeter-wave systems are commercially available and have been deployed at airports and other sites around the world. For identifying threats at larger "stand-off" distances of more than five meters, passive video imaging systems are available commercially[2] but have poor spatial and temperature resolution at frame rates faster than 5 frames per second. To achieve good noise performance at faster frame rates, several groups are developing passive imaging systems using superconducting transition edge sensors. One system with 64 detectors produces video images with a noise equivalent temperature difference (NETD) of 1.25 K at 5 Hz with a resolution of 4 cm over a 2 m × 4 m area.[3,4] Another video-imaging system has only 20 detectors but much lower noise on a per-detector basis.[5]

The millimeter and sub-millimeter astronomy community has spent the past several decades working on a similar problem: high-speed mapping of high-resolution images over a large field of view. One common solution has been the use of large-format arrays of over 1000 superconducting transition edge sensor (TES) bolometers, with multiplexed readout using superconducting quantum interference devices (SQUIDs).[6–8] The development of this technology provides the opportunity to greatly increase temperature sensitivity of terrestrial passive imaging systems.

We are developing a cryogenic passive video imaging system for operation at distances from 16 m to 28 m.[9,10] The system will contain 800 photon-noise-limited TES bolometers read out by superconducting quantum interference devices (SQUIDs) using a multiplexer developed at NIST. The system will be used as a test-bed to explore trade-offs between NETD, resolution and video frame rate, with the goal of understanding performance requirements for specific real-world stand-off imaging applications.

† Current Address: Intellectual Ventures, 11235 SE 6th St., Suite A 200, Bellevue, WA 98004

Send correspondence to Daniel Becker: E-mail: beckerd@boulder.nist.gov

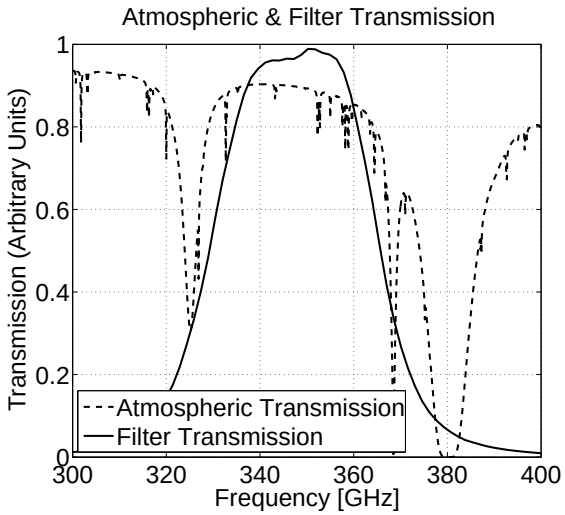

Figure 1. Plot showing measured transmission of our bandpass filter (solid lines) and typical atmospheric transmission (dashed lines). The passband is centered at approximately 350 GHz (850 μm) and has a full width at half-maximum of about 11 %.

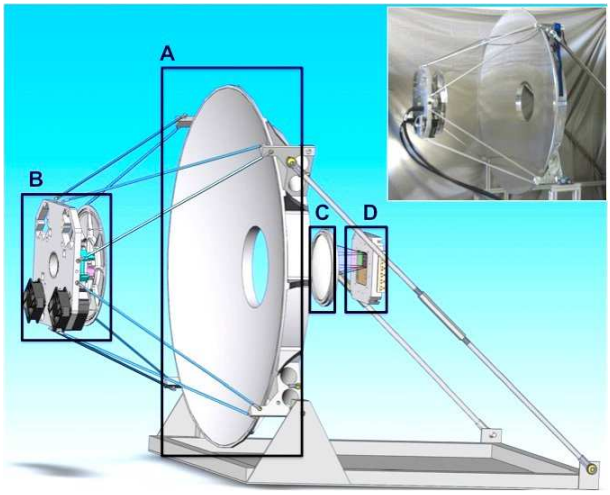

Figure 2. Schematic of optical system. Labels are (A) 1.3 m primary mirror, (B) secondary mirror with dithering mechanism, (C) cryostat window lens, (D) detector focal plane module, including bandpass filter. For clarity, the cryostat is not shown. Inset is a photograph of the primary and secondary mirror assembly.

The system will operate at a frequency of 350 GHz (850 μm) with 11 % fractional bandwidth. Spatial resolution will be 1 cm over a 1 m $\times$ 1 m field of view at a distance of 16 m, with a video rate of 20 frames per second. Measurements of prototype detectors and the system's optical efficiency indicate that the fully populated focal plane with 800 detectors should achieve NETD below 100 mK at 20 frames per second once we have optimized the optical efficiency. This paper describes the optics, detectors, readout, cryogenics and current status of this system.

2. DESIGN OVERVIEW

2.1 Optical Frequency Choice

The choice of frequency for a passive imaging system is a tradeoff between the ability to penetrate clothing (favoring low frequencies) and spatial resolution (favoring high frequencies). The 3 dB point for attenuation through clothing ranges from 350 GHz to 1 THz (high frequencies for thin materials such as Nylon, lower for thicker materials such as wool).[11] We chose 350 GHz to keep clothing attenuation at or below 3 dB and provide good spatial resolution. This frequency is also the center of an atmospheric transmission band (see Fig. 1).

2.2 Optics

Our optical system is an f/2.0 Cassegrain design. The 1.3 m elliptical primary mirror focuses light onto the hyperbolic secondary, which directs the light back through the central hole in the primary; the light then enters an ultra-high-molecular-weight (UHMW) polyethylene lens at the mouth of the cryostat. The lens makes the system telecentric, allowing use of a flat focal plane. The lens/cryostat combination can be moved relative to the primary mirror to focus the system at distances between 16 m and 28 m. The optics were simulated with ray-tracing software and shown to be diffraction-limited across the entire focal plane and at all focusing distances between 16 m and 28 m. See Fig. 2 for an annotated picture of the optical system. A detailed description of the optics has been published elsewhere.[9,10]

The observation band is defined by a metal mesh filter[12] cooled to 900 mK, defining an optical bandwidth of 40 GHz (11 % FWHM fractional bandwidth); the measured passband of this filter is shown in Fig. 1. Additional filters for thermal blocking are located at the 4 K, 50 K, and 300 K stages.[13] Total transmittance of the filter stack plus lens is predicted to be 62 %.

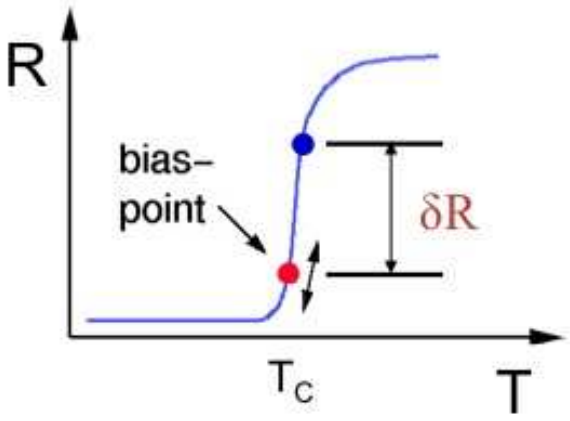

Figure 3. Illustrative plot of resistance vs temperature for a superconductor. The transition is typically very narrow, allowing the use of a superconductor as a sensitive thermometer. A TES detector is voltage-biased into the transition, with the bias point changing based on changes in optical power.

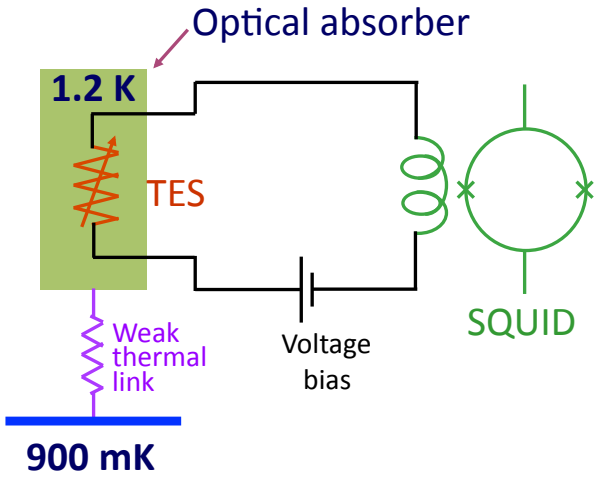

Figure 4. Schematic depiction of the operation of a TES. Optical power is absorbed onto the TES. Increases in absorbed optical power raises the temperature of the TES, raising its resistance. The dissipated V^2/R Joule power in the TES drops, compensating for the increase in optical power, leaving as constant the total dissipated power flowing out of the TES through the weak thermal link. This negative electro-thermal feedback allows the detector to operate stably. Changes in current passing through the TES are detected by a SQUID.

At the focal plane, light is captured by smooth-walled conical feedhorns that were chosen for their simplicity and ease of manufacture. To optimize coupling of the feedhorns to the rest of the optical system, we use feedhorns with a diameter of 3.2 mm, or approximately $2F\lambda$, where $F = 2.0$ is the f-number of the optics and $\lambda = 850$ μm is the optical wavelength. The taper half-angle is 9.4°, tapering to a 3.5 mm length of 0.6 mm diameter circular waveguide that leads to the detectors. The feedhorn design was modeled with finite-element electromagnetic simulations, predicting a spillover efficiency of 54 %. Conductive loss in the 3.5 mm length of 0.6 mm waveguide behind the feedhorn is calculated to be about 10 %.

At the back of the 0.6 mm circular waveguide, in front of a quarter-wave backshort, the light is absorbed by a thin-film PdAu mesh patterned on a relieved membrane, as described in section 2.4. Finite-element electromagnetic models predict that the PdAu mesh will absorb 82 % of the optical power coming down the waveguide. The mesh absorbs both polarizations.

The feedhorns will cover only a portion of the diffraction-limited area of the focal plane. Additionally, the spacing between the feedhorns is larger than the point-spread-function of the optics, so the image projected on the focal plane at any given instant will not be Nyquist sampled. Therefore, in order to use the entire diffraction-limited extent of the optics, and to generate fully sampled images, the image will be moved across the focal plane in a "dithering" pattern. This is done by moving the secondary mirror with a pair of linear actuators.

2.3 Transition Edge Sensors

Optical power is detected by voltage-biased superconducting transition edge sensor (TES) bolometers.[14,15] Below a critical temperature, T_c, a superconductor loses all resistance to DC electrical current (see Fig. 3). The sharp transition from the normal state to superconducting state allows a superconductor that has been biased into its transition to serve as a sensitive thermometer. Any signal that can be turned into a temperature change can then be detected as a change in the resistance of the superconductor. Reference 16 contains a detailed description of the behavior of TES devices.

Fig. 4 schematically depicts the operation of a voltage-biased TES bolometer. A superconducting film is thermally sunk to an optical absorber. Increased optical power raises the temperature of the film, increasing the

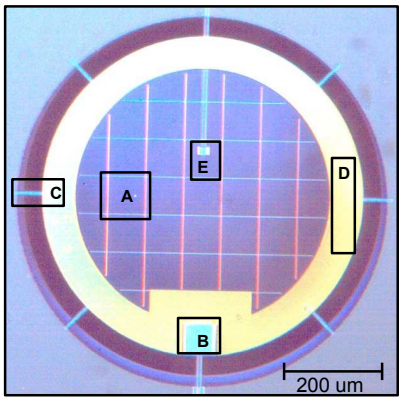

Figure 5. A picture of a prototype detector. The relieved area is 800 μm in diameter. The different components are: (A) PdAu absorbing mesh, lines 2 μm wide spaced 85 μm apart, (B) thin-film Al TES, (C) silicon nitride legs connecting relieved membrane to the bulk Si substrate that serves as low-temperature bath, (D) Au ring providing additional heat capacity to slow the thermal response time of the device for optimal readout, (E) PdAu heater resistor used for testing.

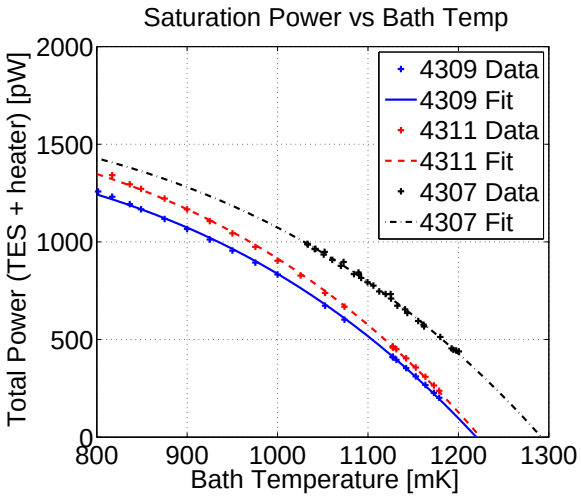

Figure 6. Plot showing saturation power $P_{\rm sat}$ vs bath temperature for three of our prototype devices. Fitting all three parameters n, K, and T_c implies $n \approx 3.6$. The fit constrains n is weakly, so for this paper we assume $n = 4.0$ everywhere; this increases our predicted detector noise by a few percent. Detector 4307 was measured in a different cryostat with different thermometry, which could explain the temperature offset from detectors 4309 and 4311.

resistance of the TES, which decreases the current passing through the circuit. A SQUID detects the drop in current. The device operates in a negative-feedback loop, with increasing optical power leading to lower V^2/R Joule heating, allowing the device to operate stably.

A weak thermal link connects the absorber and superconducting film to a low-temperature heat bath. The thermal conductance of this link determines the saturation power $P_{\rm sat}$ according to $P_{\rm sat} = K(T_c^n - T_{\rm bath}^n)$, where K and n depend on the geometry of the thermal link and the dominant heat transport mechanism in the temperature regime of interest; for our detectors we expect $n \approx 4.0$.

The dominant source of intrinsic noise in a TES bolometer is thermal fluctuations of the temperature of the TES itself. This noise is $NEP_G = F\sqrt{4k_B G T_c^2}$, where k_B is Boltzmann's constant and the differential thermal conductance G is defined as $G = dP/dT_c = nKT_c^{n-1}$. The prefactor F is unity in equilibrium, and in the range 0.5–1.0 under operating conditions.

Photon noise is also a significant source of noise in our system. The expression for photon noise, including the effect of photon bunching, is[17]

$$NEP_{\rm opt} = \sqrt{2h\nu P_{\rm opt}(1+\eta\bar{n})}, \tag{1}$$

where h is Planck's constant, ν is the central frequency, $P_{\rm opt}$ is the total optical loading, η is the optical efficiency (excluding feedhorn spillover efficiency, because the feedhorn spillover is terminated at 300 K), and $\bar{n} = [\exp(h\nu/k_BT) - 1]^{-1}$ is the average photon occupation number per mode. For our system observing 300 K radiation, $\bar{n} = 17.5$, so the bunching term is important. Total optical power per detector when observing a 300 K target will be $2\eta k_B T \Delta\nu = 165$ pW. Use of (1) then gives $NEP_{\rm opt} = 0.8$ fW/$\sqrt{\rm Hz}$.

2.4 Design of Prototype Detectors

Fig. 5 shows a picture of a prototype detector. The device is fabricated on a relieved silicon-nitride membrane approximately 800 μm in diameter. A PdAu mesh absorbs the light, with mesh dimensions (2 μm wide lines spaced 85 μm apart) chosen to match the wave impedance of the waveguide. The Al TES is at the lower edge of

the membrane and has dimensions 64 μm $\times$ 64 μm. A 15 μm $\times$ 16 μm PdAu heater resistor sits near the center of the relieved membrane for use in testing.

We designed our detectors to have $P_{\rm sat} = 1$ nW at a bath temperature of 900 mK, for a safety factor of 6 times the predicted optical loading of 165 pW. Given this saturation power, an Al TES with $T_c = 1.2$ K, a bath at 900 mK, and a target G of 4.5 nW/K should meet our NETD requirements. The dimensions of the eight silicon-nitride legs (11 μm wide $\times$ 40 μm long, 0.5 μm thick) were chosen to achieve this G.

This large thermal conductance requires a large heat capacity C to keep the thermal time constant near the 1 ms that is optimal for our readout system. We have achieved this by adding a 2 μm thick gold ring around the outer diameter of the relieved membrane.

2.5 Readout

The array is read out by the SQUID-based time-division multiplexing (TDM) system developed at NIST.[18] At room temperature a single Multi-Channel Electronics (MCE) crate will read out all 800 detectors.[19] The combination of NIST SQUID TDM with the MCE is used daily to collect data at three different millimeter-wave telescopes.[6,8,20] All hardware for the full 800 detector array, including cryogenic wiring, is already installed in our cryostat.

2.6 Cryogenics

To cool our focal plane to an operating bath temperature of 900 mK, we use a two-stage refrigeration system. The first stage is a commercially available cryogen-free cooler that reaches 3 K. The second stage is a custom-built ^{4}He sorption fridge that cools to below 1 K, and is based on a design that has been proven in the field.[21] The system reaches a base temperature of approximately 900 mK with a hold time of 13.5 hours when open optically. Operation of the cryogenics will be fully automated.

3. CURRENT STATUS

We have installed four prototype detectors into our cryostat. Individual modules with feedhorns integrated into their cover hold each detector. All data discussed in this section were taken with the complete multiplexed readout chain configured in a 2 row $\times$ 2 column format.

3.1 Dark Testing

The prototype devices have a transition temperature of approximately 1.23 K, with a normal-state resistance of about 3.5 mΩ. Fig. 6 shows measured saturation power vs. bath temperature for three tested devices; the measured G values are 5.0 nW/K to 5.4 nW/K. These values of G imply NEP_G of 0.64 fW/$\sqrt{\rm Hz}$ to 0.69 fW/$\sqrt{\rm Hz}$, assuming a prefactor F of 1.0. The measured NEP under no optical load for a prototype detector is shown in Fig. 7. The measured noise level matches the prediction well.

Adding the measured detector noise and predicted photon noise in quadrature gives $NEP_{\rm tot} = 1.1$ fW/$\sqrt{\rm Hz}$. This total NEP can be converted to an NETD through the use of the radiometer equation,[22]

$$NETD = \frac{NEP_{\rm tot}}{2k_B\Delta\nu\eta\sqrt{2\tau}}, \tag{2}$$

where τ is the total integration time per pixel in the processed video frame, $\Delta\nu = 40$ GHz is the pre-detection optical bandwidth, and $\eta = 0.25$ is the total optical efficiency (0.82 absorber efficiency, 0.62 filter stack efficiency, 0.54 feedhorn spillover efficiency and 0.90 feedhorn insertion loss). Creating a 1 m^2 image with 1 cm resolution requires 200^2 pixels per video frame. With an 800 detector system, this leads to a "dithering factor" of $200^2/800 = 50$, meaning that each detector will image 50 image pixels per video frame, and $\tau = 1/(50)(20$ Hz). Equation 2 thus predicts that our system will have $NETD = 85$ mK across the full field of view at 20 FPS.

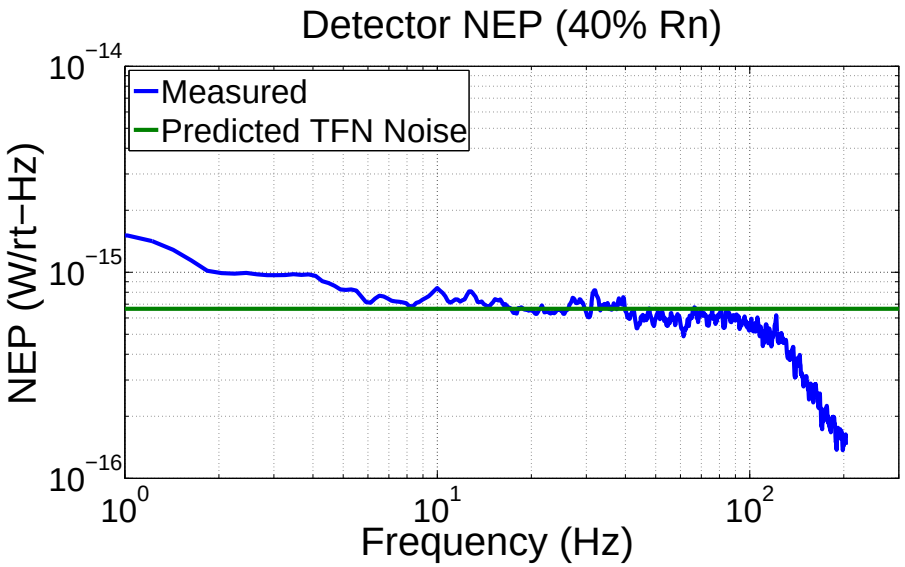

Figure 7. Plot showing measured noise equivalent power (NEP) spectral density for a prototype detector, under no optical load. The white noise level is about 0.65 fW/$\sqrt{\text{Hz}}$. The low-frequency increase in noise is due to a drift in bath temperature that we are fixing. The 120 Hz rolloff is due to a filter in the readout electronics that was turned on while acquiring this spectrum.

3.2 Optical Testing

Our optical testing has focused on two areas: measuring optical efficiency and taking still images.

To measure total optical efficiency we measure the difference in detected optical power between when the imager is observing 295 K and 77 K blackbodies. If this difference in detected optical power is $\Delta P_{295/77}$, then the total optical efficiency of the system is defined as $\left(\Delta P_{295/77}\right) / \left(2 k_B \Delta T \Delta \nu\right)$. The 295 K blackbody is a sheet of room-temperature Eccosorb AN-72 attached to an aluminum backing sheet. The 77 K blackbody is a sheet of Eccosorb AN-72 submerged in liquid nitrogen held in a styrofoam cooler with walls approximately 2.5 cm thick. We apply a correction to account for the imperfect transmission of the styrofoam cooler's walls, which we measured by moving the cooler's lid back and forth in front of the cooler. This measurement approach resulted in an average optical efficiency of 11.5 % for the four detectors, about half of the predicted value of 26 %. We have not yet identified the source of the lost efficiency, but it is likely that some of the loss is due to poor alignment of the cryostat with the primary and secondary mirrors.

We do not yet have enough detectors installed to take video images. But we can take still images by using the secondary mirror to raster scan over the target. Fig. 8 shows an image of a person with a ceramic knife concealed beneath his shirt. This image includes data from three detectors, with a large area of overlap near the image center. The knife is visible on the left side. Also visible is the outline of a pocket, the shirt collar, and the strip of extra cloth backing the shirt's buttons.

To produce this image, we combined data simultaneously acquired by three detectors. First, data from each detector were used to create three sub-images. Second, an edge taper was applied to each sub-image, and all three sub-images were combined. Third, the full image was Weiner deconvolved by use of the measured point-spread-function of the system, which has the effect of both (a) reducing noise on spatial scales smaller than the system's resolution, and (b) improving apparent resolution.

The temperature scale was calibrated by use of the heaters and the measured optical efficiency. The expected contrast in the image is 12 K (skin temperature of 310 K with emissivity of 0.80, lab background temperature of 295 K). The total contrast in the image is 14 K, indicating that the calibration is reasonable. We estimate the image NETD by taking the standard deviation of pixel temperature values in a flat area of each sub-image. This yields an NETD of 85 mK, which is about what we expect, given the integration time per sub-image pixel of 5.5 ms and the measured optical efficiency. The integration time per pixel for video images will be 1 ms, so

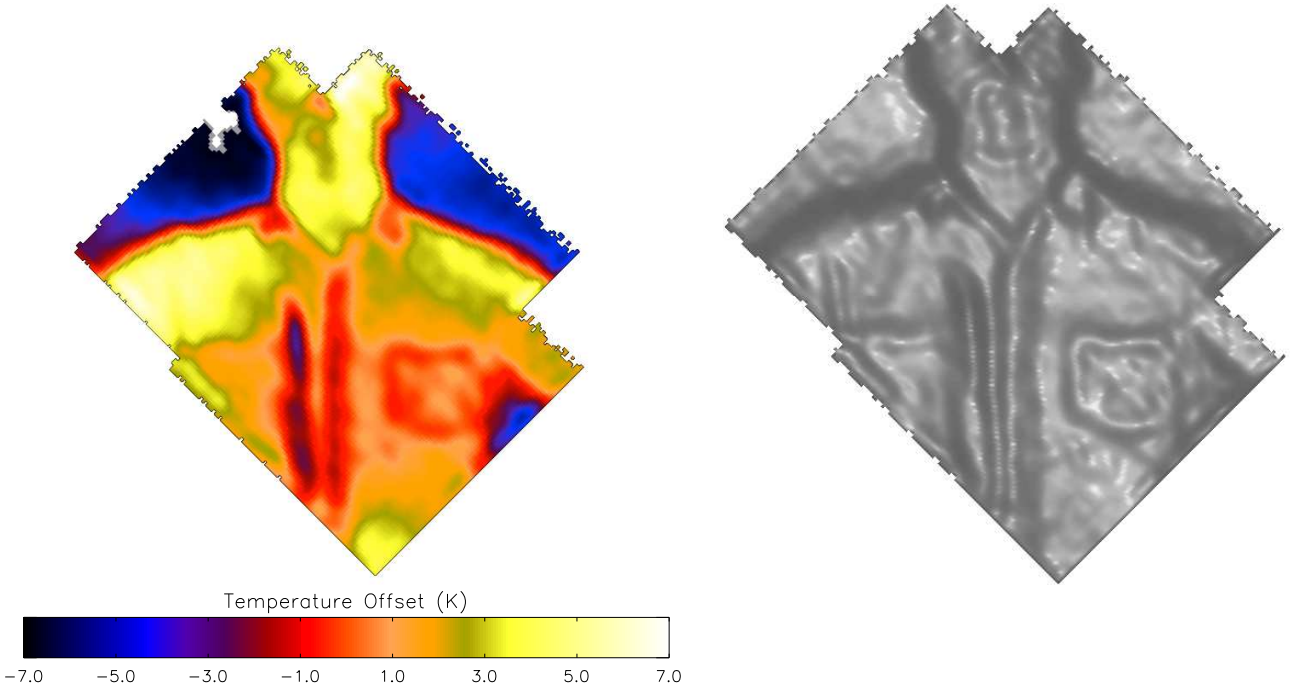

Figure 8. Two representations of a still image taken with our system. The image was taken by raster scanning across a person with a ceramic knife concealed beneath his shirt. The knife is visible on the left side of each image. Also visible is the outline of a pocket, the shirt collar, and the strip of extra cloth backing the shirt's buttons. The total time to acquire the image was 50 s, with an average of 5.5 ms integration time per image pixel. **Left** False-color temperature mapping. The video-rate NETD implied by this image is 200 mK, which can be reduced to below 100 mK through optimization of the optical system. The total contrast in the image is 14 K, and the contrast between the knife and the warm part of the body next to it is 3.9 K. **Right** "Topographic" mapping of the same image data. The data is plotted as a 3-D image, lit from directly above by a light source, and viewed from directly above. This 3-D representation is routinely used with range data in active radar imaging systems.[23]

the implied NETD for video rate images is 85 mK $\times \sqrt{5.5} = 200$ mK. This is approximately two times higher than predicted in section 3.1, which is expected because of our poor measured optical efficiency. Optimization of the optics should allows us to reach the predicted 85 mK NETD.

4. NEXT-GENERATION SYSTEM

The current system features high sensitivity and low noise to facilitate the investigation of the tradeoffs inherent in an operational system. Adapting this system for field deployment will require reduction in cost, weight, and complexity. In addition to modifications such as molded composite optical elements and simplified cryogenics, we are planning to read out a next-generation system with gigahertz micro-resonators that can read out focal planes of either TESs or Microwave Kinetic Inductance Devices (MKIDs).[24] This technology can read out hundreds of detectors with a single coaxial cable, greatly reducing the cost and complexity of cryogenic wiring, and allowing focal planes with larger numbers of detectors.

5. CONCLUSION

We have designed a 350 GHz cryogenic terrestrial passive video imaging system by leveraging technology proven in the millimeter and sub-millimeter astronomy fields. The video imager will use 800 TES bolometers to image a 1 m $\times$ 1 m field to a resolution of 1 cm at a distance of 16 m at video frame rates. Measurements of our prototype detectors indicate that they are close to being photon-noise-limited. Initial optical testing indicates that the fully populated system will take video-rate images with 200 mK NETD. Improving NETD to the predicted 85 mK requires optimizing our optical efficiency, but requires no changes to the detector design. Our next steps are to design, fabricate, and install the full 800-detector focal plane.

REFERENCES

[1] R. Appleby, "Passive millimetre–wave imaging and how it differs from terahertz imaging," *Philosophical Transactions A* **362**(1815), p. 379, 2004.

[2] C. Mann, "First demonstration of a vehicle mounted 250GHz real time passive imager," in *Proceedings of SPIE*, **7311**, p. 73110Q, 2009.

[3] A. Luukanen and J. Pekola, "A superconducting antenna-coupled hot-spot microbolometer," *Applied Physics Letters* **82**, p. 3970, 2003.

[4] E. Grossman, C. Dietlein, J. Ala-Laurinaho, M. Leivo, L. Gronberg, M. Gronholm, P. Lappalainen, A. Rautiainen, A. Tamminen, and A. Luukanen, "Passive terahertz camera for standoff security screening," *Applied optics* **49**(19), pp. E106–E120, 2010.

[5] E. Heinz, D. Born, G. Zieger, T. May, T. Krause, A. Krüger, M. Schulz, S. Anders, V. Zakosarenko, H. Meyer, *et al.*, "Progress report on Safe VISITOR: approaching a practical instrument for terahertz security screening," in *Proceedings of SPIE*, **7670**, p. 767005, 2010.

[6] D. Swetz, P. Ade, C. Allen, M. Amiri, J. Appel, E. Battistelli, B. Burger, J. Chervenak, A. Dahlen, S. Das, *et al.*, "Instrument design and characterization of the millimeter Bolometer Array Camera on the Atacama Cosmology Telescope," in *Proceedings of SPIE*, **7020**, p. 702008, 2008.

[7] J. Ruhl, P. Ade, J. Carlstrom, H. Cho, T. Crawford, M. Dobbs, C. Greer, N. Halverson, W. Holzapfel, T. Lanting, *et al.*, "The south pole telescope," in *Proceedings of SPIE*, **5498**, pp. 11–29, 2004.

[8] W. Holland, W. Duncan, B. Kelly, K. Irwin, A. Walton, P. Ade, and E. Robson, "SCUBA-2: a large-format submillimeter camera on the James Clerk Maxwell Telescope," in *Proceedings of SPIE*, **4855**, p. 1, 2003.

[9] W. Duncan, R. Schwall, K. Irwin, J. Beall, C. Reintsema, W. Doriese, H. Cho, B. Estey, G. Chattopadhyay, P. Ade, *et al.*, "An Optical System for Body Imaging from a Distance Using Near-TeraHertz Frequencies," *Journal of Low Temperature Physics* **151**(3), pp. 777–783, 2008.

[10] D. Becker, J. Beall, H. Cho, W. Duncan, G. Hilton, R. Horansky, K. Irwin, P. Lowell, M. Niemack, N. Paulter, *et al.*, "A 350-GHz high-resolution high-sensitivity passive video imaging system," in *Proceedings of SPIE*, **7670**, p. 76700M, 2010.

[11] J. Bjarnason, T. Chan, A. Lee, M. Celis, and E. Brown, "Millimeter-wave, terahertz, and mid-infrared transmission through common clothing," *Applied Physics Letters* **85**(4), pp. 519–521, 2004.

[12] P. Ade, G. Pisano, C. Tucker, and S. Weaver, "A review of metal mesh filters," in *Proceedings of SPIE*, **6275**, pp. 62750U–1, 2006.

[13] C. Tucker and P. Ade, "Thermal filtering for large aperture cryogenic detector arrays," in *Proceedings of SPIE*, **6275**, p. 62750T, 2006.

[14] K. Irwin, "An application of electrothermal feedback for high resolution cryogenic particle detection," *Applied Physics Letters* **66**, p. 1998, 1995.

[15] A. Lee, P. Richards, S. Nam, B. Cabrera, and K. Irwin, "A superconducting bolometer with strong electrothermal feedback," *Applied Physics Letters* **69**, p. 1801, 1996.

[16] K. D. Irwin and G. C. Hilton, *Cryogenic Particle Detection*, ch. Transition Edge Sensors, pp. 63–149. Springer-Verlag Berlin Heidelberg, 2005.

[17] J. Zmuidzinas, "Thermal noise and correlations in photon detection," *Applied optics* **42**(25), pp. 4989–5008, 2003.

[18] P. de Korte, J. Beyer, S. Deiker, G. Hilton, K. Irwin, M. MacIntosh, S. Nam, C. Reintsema, L. Vale, and M. Huber, "Time-division superconducting quantum interference device multiplexer for transition-edge sensors," *Review of Scientific Instruments* **74**, p. 3807, 2003.

[19] E. Battistelli, M. Amiri, B. Burger, M. Halpern, S. Knotek, M. Ellis, X. Gao, D. Kelly, M. Macintosh, K. Irwin, *et al.*, "Functional description of read-out electronics for time-domain multiplexed bolometers for millimeter and sub-millimeter astronomy," *Journal of Low Temperature Physics* **151**(3), pp. 908–914, 2008.

[20] R. Ogburn IV, P. Ade, R. Aikin, M. Amiri, S. Benton, J. Bock, J. Bonetti, J. Brevik, B. Burger, C. Dowell, *et al.*, "The BICEP2 CMB polarization experiment," in *Proceedings of SPIE*, **7741**, p. 77411G, 2010.

[21] M. Devlin, S. Dicker, J. Klein, and M. Supanich, "A high capacity completely closed-cycle 250 mK 3He refrigeration system based on a pulse tube cooler," *Cryogenics* **44**(9), pp. 611–616, 2004.

[22] R. Dicke, "The measurement of thermal radiation at microwave frequencies," *Review of Scientific Instruments* **17**(7), pp. 268–275, 1946.

[23] K. Cooper, R. Dengler, N. Llombart, T. Bryllert, G. Chattopadhyay, E. Schlecht, J. Gill, C. Lee, A. Skalare, I. Mehdi, *et al.*, "Penetrating 3-D imaging at 4-and 25-m range using a submillimeter-wave radar," *Microwave Theory and Techniques, IEEE Transactions on* **56**(12), pp. 2771–2778, 2008.

[24] B. Mazin, P. Day, K. Irwin, C. Reintsema, and J. Zmuidzinas, "Digital readouts for large microwave low-temperature detector arrays," *Nuclear Instruments and Methods in Physics Research Section A: Accelerators, Spectrometers, Detectors and Associated Equipment* **559**(2), pp. 799–801, 2006.